Strategies for residue explosives detection using laser-induced breakdown spectroscopy†

Jennifer L. Gottfried,* Frank C. De Lucia, Jr, Chase A. Munson and Andrzej W. Miziolek

Received 15th March 2007, Accepted 5th October 2007
First published as an Advance Article on the web 22nd October 2007
DOI: 10.1039/b703891g

The ability to detect trace amounts of explosives and their residues in real time is of vital interest to Homeland Security and the military. Previous work at the US Army Research Laboratory (ARL) demonstrated the potential of laser-induced breakdown spectroscopy (LIBS) for the detection of energetic materials. Our recent efforts have been focused on improving the sensitivity and selectivity of LIBS for residue explosives detection and on extending this work to the standoff detection of explosive residues. One difficulty with detecting energetic materials is that the contribution to the oxygen and nitrogen signals from air can impede the identification of the explosive material. Techniques for reducing the air entrainment into the plasma—such as using an argon buffer gas or a collinear double-pulse configuration—have been investigated for this application. In addition to the laboratory studies, ARL's new double-pulse standoff system (ST-LIBS) has recently been used to detect explosive residues at 20 m. The efficacy of chemometric techniques such as linear correlation, principal components analysis (PCA), and partial least squares discriminant analysis (PLS-DA) for the identification of explosive residues is also discussed. We have shown that despite the typical characterization of LIBS as an elemental technique, the relative elemental intensities in the LIBS spectra are representative of the stoichiometry of the parent molecules and can be used to discriminate materials containing the same elements. Simultaneous biohazard and explosive residue discrimination at standoff distances has also been demonstrated.

Introduction

The detection of explosives for security screening, demining, environmental decontamination and other applications relevant to Homeland Security is an active area of research. While some methods for detecting bulk explosives such as X-ray analysis, neutron activation or scattering (which measures quantities of carbon, nitrogen, and oxygen),[1] and terahertz imaging are currently used or under development, many of these systems are quite large and expensive. One of the most pressing needs for the military is the standoff detection of explosives. Techniques such as X-ray imaging and neutron activation suffer from reduced sensitivity at increasing distances and generate harmful ionizing radiation, making them poor candidates for standoff detection.[2] Although terahertz imaging is a promising technique utilizing non-ionizing radiation, absorption of water vapor and other species in the atmosphere can potentially limit its application to standoff detection.[3]

Most trace explosives detection techniques such as ion mobility spectrometry and gas chromatography rely on vapor detection. Unfortunately, at room temperatures the vapor pressures of many common explosives are extremely small (ppb_v or less) and attempts to conceal the explosives by sealing them in packaging materials can decrease the vapor concentrations by up to three orders of magnitude.[4] A study by Gresham *et al.*,[5] however, showed that a series of successive thumb prints laid down sequentially on a sample target resulted in RDX residue contamination on the order of several milligrams for a first generation C-4 fingerprint and nanogram level contamination for the 40th to 50th print. Optical techniques such as cavity ringdown spectroscopy (CRDS), Raman spectroscopy, photoacoustic spectroscopy, and photofragmentation followed by resonance-enhanced multiphoton ionization (PF–REMPI) or laser-induced fluorescence (PF–LIF) have been applied to trace explosive detection.[6] Of these techniques, only Raman has been demonstrated on solid explosives at standoff distances (10–50 m), although long integration times (*i.e.* multiple laser shots) were required to improve the signal-to-noise.[7,8]

An alternative optical technique for the detection of explosives is laser-induced breakdown spectroscopy (LIBS). LIBS is a spectroscopic analysis technique that uses the light emitted from a laser-generated microplasma to determine the composition of the sample based on elemental and molecular emission intensities. LIBS provides real-time detection of solids, liquids, and vapors without the need for sample preparation. Previous work at the US Army Research Laboratory (ARL) demonstrated the potential of LIBS for close-contact bulk

US Army Research Laboratory, AMSRD-ARL-WM-BD, Aberdeen Proving Ground, MD, 21005-5069, USA. Fax: +1-410-306-1909; Tel: +1-410-306-0884. E-mail: jennifer.gottfried@arl.army.mil
† The HTML version of this article has been enhanced with colour images.

Table 1 Molecular formulas for common explosives and potential interferents

Explosive	Formula	Potential interferent	Formula
RDX	$C_3H_6N_6O_6$	Polyurethane	$C_{17}H_{15}O_4N_2$
TNT	$C_7H_5N_3O_6$	Methyl-2-cyanoacrylate	$C_5H_5O_2N$
PETN	$C_5H_8N_4O_{12}$	Diesel fuel	$C_{10}H_{22}$-$C_{15}H_{32}$
HMX	$C_4H_8N_8O_8$	Oils (fatty acids)	$CH_3(CH_2)_2COOH$, $CH_3(CH_2)_{18}COOH$

energetic materials detection.[9] The discrimination and identification of plastic landmine casings using LIBS has also been demonstrated.[10] One of the biggest advantages of LIBS is the simplicity and ruggedness of the instrumentation. Both man-portable (MP-LIBS)[11] and standoff LIBS (ST-LIBS)[12] devices have been developed by ARL with industrial partners and successfully tested on a variety of hazardous materials including explosives, biological agent surrogates, and chemical weapon simulants.

Recent efforts at ARL have been focused on improving the sensitivity and selectivity of LIBS for the detection of explosive residues. The ability of LIBS to detect trace amounts of materials with a single laser shot is especially important for residue detection, since the first shot can ablate all or most of the residue. Table 1 lists the molecular formulas for common military explosives and potential organic interferents. Since most energetic materials contain higher concentrations of oxygen and nitrogen compared to the carbon and hydrogen in non-energetic organic materials, explosive residues can be distinguished from non-energetic materials based on the elemental ratios of those species. However, entrainment of atmospheric oxygen and nitrogen into the laser-induced plasma complicates the discrimination of energetic and non-energetic materials. The use of argon as a buffer gas in order to eliminate the contribution of oxygen and nitrogen from air in the LIBS signal and collinear double-pulse LIBS have been evaluated for close-contact and standoff detection of explosive residues.

Experimental

Explosive samples of research grade RDX, TNT and Composition-B (36% TNT, 63% RDX, and 1% wax) were provided by our colleagues at the US Army Research Laboratory. For residue detection, *ca.* 4–5 mg of the powdered forms of the pure explosives was dissolved in *ca.* 3 mL of acetone and applied to a heavy duty aluminium foil substrate using a 10 μL syringe.

The interferent Arizona road dust was provided by Battelle and applied to the aluminium foil in a very thin layer. A commercial lubricant (WD-40®) was used as an oil interferent. A small amount was sprayed on the aluminium substrate, then wiped almost completely off with a clean-room cloth. Fingerprint residue was applied by repeatedly handling the surface of the aluminium with clean hands (depositing oil from the surface of the skin in a fingerprint pattern). The aluminium foil samples were used straight from the roll without additional cleaning. Each residue type was prepared on several pieces of aluminium foil, and the collected LIBS spectra were acquired from laser shots evenly distributed among the foil samples.

RDX and dust mixtures (50% w/w) were prepared using two methods. For the first method, 2.5 mg of RDX and 2.5 mg of Arizona dust were suspended in 3 mL of acetone. The solution was thoroughly mixed and quickly applied to the aluminium foil using a 10 μL syringe. Although this method provides a homogeneous mixture, it does not represent 'real-world' conditions so a second method was employed. A thin layer of Arizona dust was applied to the aluminium foil and several milligrams of RDX powder was crushed onto the surface (*ca.* 60 cm^2), creating an inhomogeneous mixture. Oil and dust mixtures were similarly prepared by smearing a clean-room cloth soaked with oil on a thin layer of dust.

The anthrax surrogate *Bacillus subtilis* var. *niger* (commonly known as *Bacillus globigii*, or BG) and mold sample *Alternia alternata* (AA) were provided by Battelle. The residue samples of the biomaterials were prepared in an analogous manner to the explosives residues (*ca.* 4–5 mg dissolved in 3 mL of acetone).

Spectra of the prepared samples were acquired using a portable MP-LIBS backpack system, a laboratory double-pulse LIBS system (described in detail elsewhere[13]), and a standoff double-pulse LIBS system. ARL and partners have developed several generations of MP-LIBS systems in conjunction with Ocean Optics, Inc. These devices have previously been applied to mine detection and biological and chemical warfare agent simulant detection.[14–16]

In conjunction with Applied Photonics Ltd and Ocean Optics, ARL has developed a standoff LIBS system (ST-LIBS) that uses a collinear double-pulse configuration based on the Quantel Brilliant Twins laser system (1064 nm, 10 Hz, 335 mJ per pulse, 5 ns pulse width). Detection of metals, bulk explosives, plastics, bulk biomaterials, and chemical nerve agent simulants at 20 m has previously been demonstrated using this system.[12] In that initial study we demonstrated the potential of standoff LIBS for explosive residue discrimination using principal components analysis (PCA). We have extended these studies to evaluate the ability of the ST-LIBS system to discriminate explosive residues from a wider range of interferents, including biomaterials and explosive-containing mixtures. We have also performed, for the first time, a comprehensive evaluation of various chemometric techniques for explosive detection with standoff LIBS.

Linear correlation analysis of the total ST-LIBS spectra (190–840 nm, *ca.* 0.1 nm resolution) and specific peak intensities and ratios was performed using the data analysis feature of Microsoft Excel. PCA, soft independent method of class analogy (SIMCA), and partial least squares discriminant analysis (PLS-DA) models were generated using the PLS_Toolbox version 3.5 (Eigenvector Technologies, Inc.) running under Matlab version 7.0 (Mathworks). The data were auto-scaled prior to building the models.

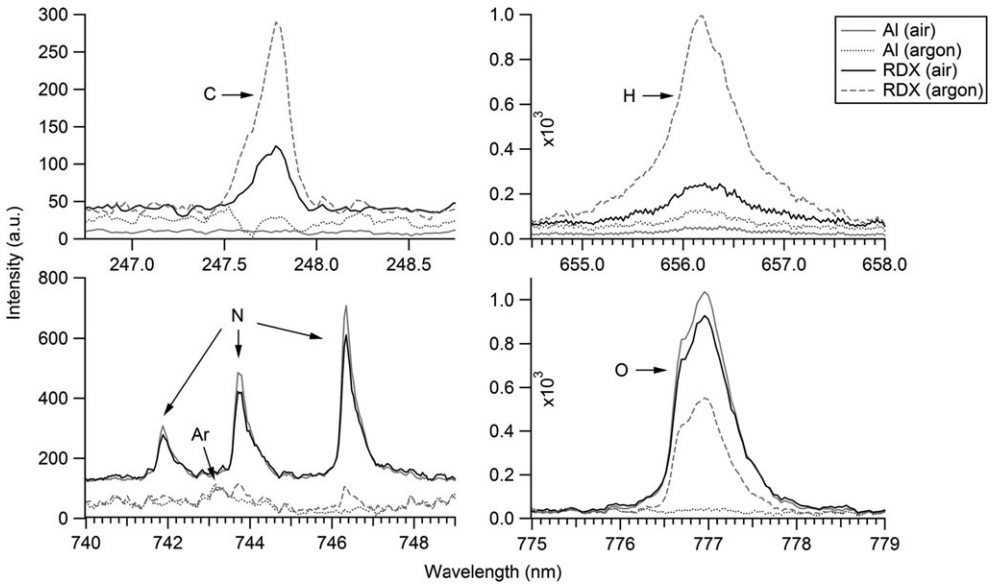

Fig. 1 Single-shot spectra of aluminium and RDX residue on Al in air and under argon acquired using the MP-LIBS system. Approximately 400 ng mm^{-2} of RDX was applied to the aluminium foil substrate, and ten spectra of each sample under each condition were acquired. The C (247 nm) and H (656 nm) signals from the RDX are enhanced under argon, while the O (777 nm) and N (742–747 nm) signals under argon are representative of the sample composition rather than atmospheric contributions.

Results

The single-shot spectra in Fig. 1 were acquired using an MP-LIBS system with *ca.* 25 mJ per laser pulse (1064 nm, *ca.* 7 ns). An argon flow was directed across the sample region and ten spectra of the aluminium substrate and RDX (*ca.* 400 ng mm^{-2}) were acquired. Air spectra were also obtained for comparison. The addition of argon to the LIBS plasma enhances the C (247.856 nm) and H (656.285 nm) lines, increasing the sensitivity of the MP-LIBS system. When argon is used to displace the air the N (742.364, 744.229, and 746.831 nm) and O (777.194/777.417 nm) lines are representative of the sample composition rather than atmospheric contributions to the signal.

Fig. 2 compares the background-corrected peak height intensity ratio of the oxygen (777.417 nm) to nitrogen (746.831 nm) lines for the four samples (Al in air, RDX on Al in air, Al in argon, and RDX on Al in argon). For the Al sample, O/N is indicative of the amount of oxygen relative to nitrogen in the atmosphere, since the sample itself contains no oxygen or nitrogen (except possibly from trace surface contamination). The RDX residue, on the other hand, contains more oxygen relative to nitrogen than air. The separation of the O/N values for Al and RDX based on the 95% confidence intervals is much larger for the two samples under argon than it is in air because of the decrease in the amount of air entrained in the plasma with the argon flow. These results show that for low pulse powers (single pulse) the use of argon is essential for improving the selectivity of the MP-LIBS system for explosive residue detection.

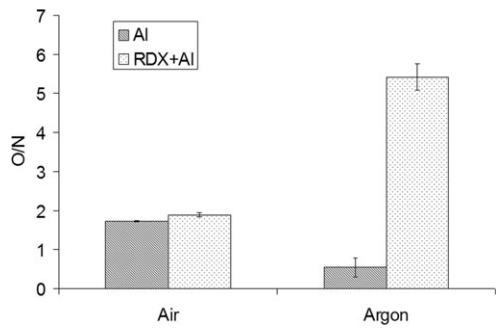

Fig. 2 Relative oxygen to nitrogen peak intensities for aluminium and RDX residue on aluminium in air and in an argon flow (error bars represent the 95% confidence interval for the ten spectra acquired using the MP-LIBS system). The RDX residue can be most easily discriminated from the aluminium substrate (using the O/N ratio) under argon.

We have also investigated the use of argon as a buffer gas for explosive residue detection using higher laser powers with a laboratory LIBS system based on a Continuum Surelite collinear double-pulse laser system. The system is operated in single-shot mode with an interpulse separation $\Delta t = 2$ μs. The flashlamps continuously fire at 5 Hz. Under these conditions, each laser can deliver up to 320 mJ per pulse at 1064 nm (*ca.* 8 ns pulse width). Twenty single-pulse (320 mJ) and twenty double-pulse (2 × 160 mJ) spectra of aluminium and RDX residues were acquired in air and with an argon flow directed across the sample region. Fig. 3 compares the O/N ratios for each sample. The average O/N ratios for single-pulse Al and RDX residue spectra in air overlap significantly (within the 95% confidence intervals) as a result of the atmospheric contribution to the O and N signals. The use of an argon flow to displace the air results in a separation of the O/N values for the Al and RDX residue.

Although these results confirm the necessity of using argon for single-pulse LIBS detection of explosive residues, the ideal detector would be capable of standoff detection of explosive

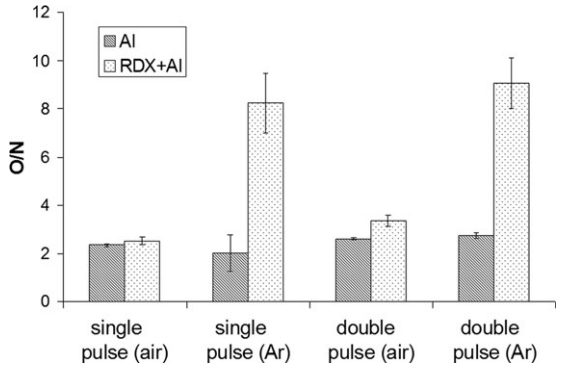

Fig. 3 Comparison of the reduction in air entrainment using a single 320 mJ pulse under an argon flow *versus* using a double laser pulse (with an interpulse separation Δt = 2 μs and total energy = 320 mJ). Twenty spectra of the aluminium and RDX residue samples in air and under an argon flow were acquired with the Continuum Surelite lasers using our laboratory LIBS setup. The oxygen to nitrogen ratios for a single 320 mJ pulse in air (maximum air entrainment) and a double laser pulse under an argon flow (minimal air entrainment) are also shown for comparison. The aluminium and RDX residue can be discriminated based on O/N (with 95% confidence intervals) when an argon flow and/or a double pulse is used (*i.e.* the O/N values for the two samples do not overlap); using double-pulse LIBS in air provides smaller standard deviations than single-pulse LIBS under argon.

residues from tens to hundreds of meters. An argon flow cannot practically be delivered to the sample surface for standoff applications. Double-pulse LIBS has been extensively investigated because of the signal enhancement attributable to the greater mass ablation and increase in plasma volume caused by the reduced density environment following the first laser pulse.[17] Fig. 3 shows that separation of the O/N ratios for the Al and RDX samples can also be achieved using collinear double pulses. Although the separation between the samples is not as large as with the argon flow (since displacement of the air is not complete), the standard deviation of the measurements is significantly lower using a double pulse in air rather than the single pulse with argon. The combination of double-pulse LIBS with an argon flow results in large separation of the O/N ratios for the two samples as well as slightly lower standard deviations.

Fig. 4 compares the single- *vs.* double-pulse LIBS spectra of RDX residue using the laboratory system (with a Catalina Echelle/Andor i-Star ICCD spectrometer) and the ST-LIBS system (with a three-channel gated CCD spectrometer by Ocean Optics). Although the close-contact double-pulse spectrum shows some signal enhancement over the single-pulse spectrum, the increase in emission intensity is not as dramatic as that seen for the standoff double-pulse spectrum. In addition to strong enhancement of the aluminium lines from the substrate, the C, H, N, and O lines are also enhanced by a factor of 2–3. Fig. 5 shows the relative O/C, O/N, and N/C ratios for RDX residue spectra acquired with the ST-LIBS system at 20 m as a function of interpulse delay (averaged values for 20 spectra with 95% confidence intervals). The O/C and N/C ratios are minimized at Δt = 3 μs, while O/N reaches a maximum. This indicates that the air entrained into the plasma is minimized at the optimal interpulse separation of Δt = 3 μs. The statistical overlap between the ratios for the different interpulse delays suggests that any interpulse delay >3 μs (at least up to 10 μs) may work equally as well for explosive discrimination on an aluminium substrate, although the overall emission intensity does begin to decrease at longer interpulse delays.

Using the optimized timing for the ST-LIBS system (delay time t_{delay} = 2 μs, integration time gate t_{int} = 100 μs, and interpulse separation Δt = 3 μs), 50 spectra were acquired at 20 m (*ca.* 550 mJ total laser energy) for each of the sample

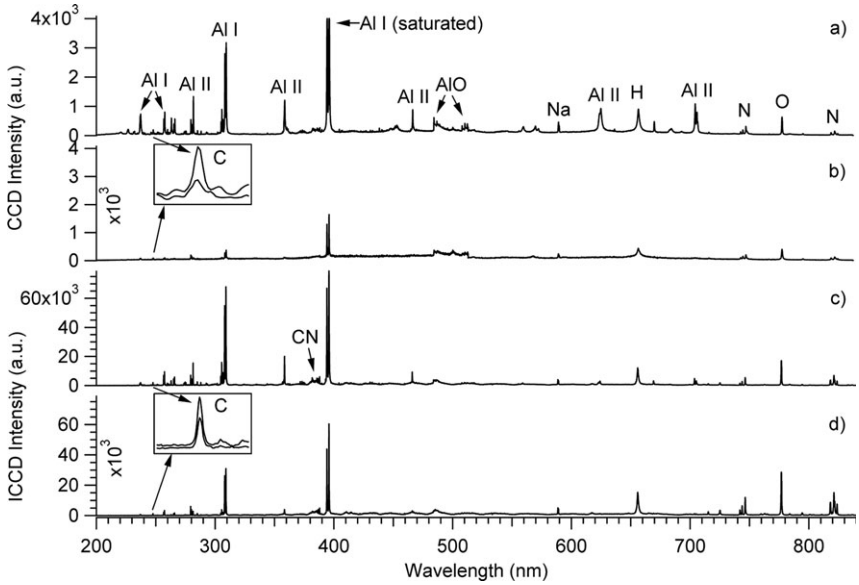

Fig. 4 LIBS spectra (20 shots averaged) of RDX residue on Al (a) at 20 m with a double-pulse laser (275 mJ total energy, Δt = 3 μs, CCD spectrometer), (b) at 20 m with a single 275 mJ pulse, (c) at close-contact with a double-pulse laser (320 mJ total energy, Δt = 2 μs, ICCD spectrometer), and (d) at close-contact with a single 320 mJ pulse. Strong emission lines are labeled for reference and the C line at 247 nm is inset and magnified on a 2 nm scale.

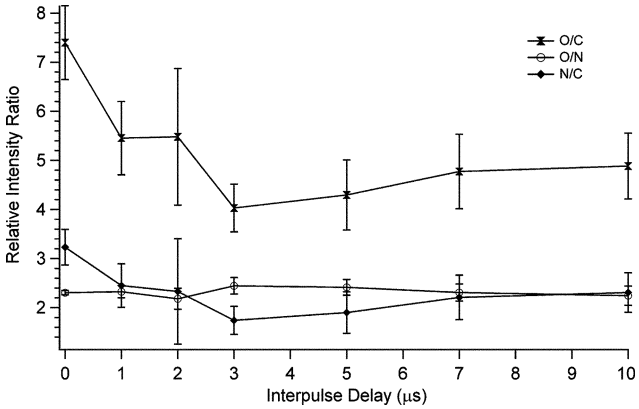

Fig. 5 Relative intensities (O/C, O/N, N/C) *versus* interpulse separation for RDX residue sample spectrum acquired at 20 m. Values are averaged over 20 spectra with 95% confidence intervals. The optimal delay between pulses occurs at $\Delta t = 3$ μs, where the O/C and N/C ratios are minimized and the O/N ratio is maximized, indicating minimal air entrainment.

types described in the Experimental section. Fig. 6 shows the single-shot spectra of each of the interferents and a representative explosive residue (TNT). In addition to the Al I–II and AlO emission caused by ablation of the aluminium substrate, the explosive residue spectra contain C, CN, Ca, C_2, Na, H, N, K, and O lines. Calcium, sodium and potassium were the only impurities observed in the explosives spectra. Differences in the broadband spectra shown in Fig. 6 are difficult to pick out without the aid of chemometric techniques, since many of the substances contain the same elements. Because the spectra were acquired using a double-pulse laser which reduces background signals from the air, key ratios of the elements found in explosives can be used to discriminate the different samples. The following section discusses the effectiveness of different chemometric techniques for explosives discrimination using LIBS spectra.

Analysis

While the double-pulse ST-LIBS results discussed in the previous section demonstrate the detection of explosive residues at standoff distances using LIBS, the discrimination of explosive and non-explosive residues requires further analysis. The ideal technique would provide low false negative rates for the detection of explosive samples and low false positive rates for non-explosive samples. In addition, the technique should be capable of correctly classifying unknown samples not incorporated in the model as explosive or non-explosive and successfully identifying explosive-containing mixtures. We have investigated the discrimination ability of our system using techniques such as flowchart analysis, linear correlation, principal components analysis, soft independent method of class analogy, and partial least squares discriminant analysis.

In an initial field test of an early standoff LIBS system developed by the Laserna group at the University of Málaga,[18] a flowchart algorithm was developed to decide whether a sample was an explosive or a non-explosive. All of the blind test samples were correctly identified using the data processing algorithm. A similar algorithm based on 16 conditions describing relative emission intensities was developed and applied to the residue data collected with ARL's ST-LIBS system. In contrast to the Málaga algorithm, none of the criteria depend on specific numbers. If all of the following conditions are true (O/C > N/C, O/C > N/CN, H/C > O/H,

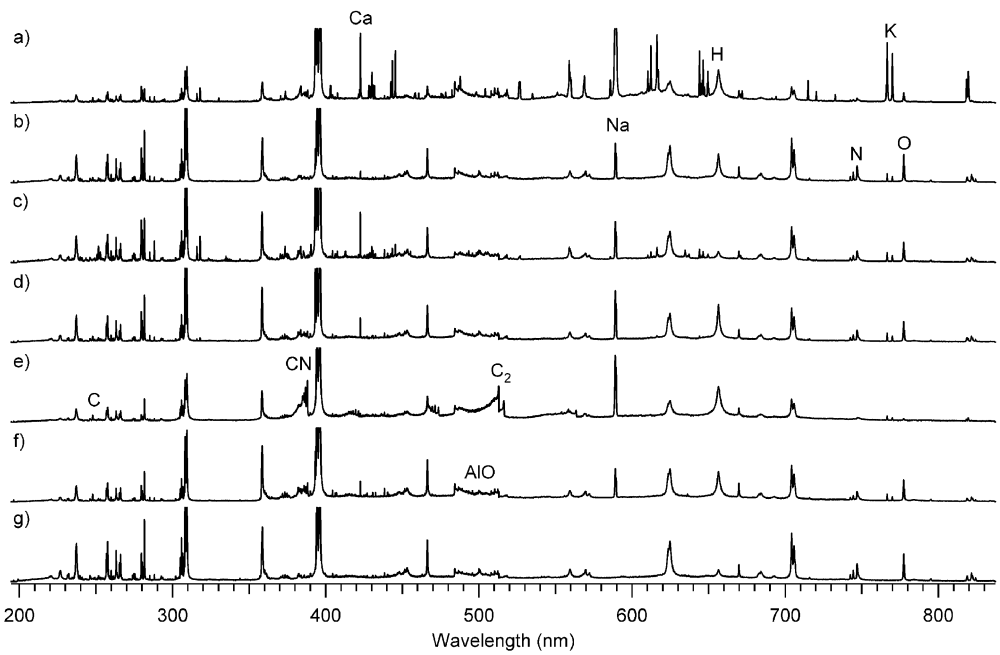

Fig. 6 Single-shot spectra (ST-LIBS at 20 m, *ca.* 550 mJ total energy) of various residues on an aluminium substrate: (a) *Bacillus subtilis* (anthrax surrogate), (b) *Alternia alternata* (mold), (c) Arizona dust, (d) fingerprint residue, (e) lubricant oil, (f) TNT, and (g) aluminium substrate. Strong emission lines of C, CN, Ca, AlO, C_2, Na, H, N, K, and O are labeled in the spectra. Differences in the spectra are difficult to see by eye (especially with the aluminium background), but can be efficiently revealed using chemometric techniques.

Table 2 Lines from the explosives spectra used for the discrimination of sample residues (the background-corrected peak intensities of each atomic/molecular species were added to give summed peak intensities for C, C_2, CN, H, N, O, Ca, Na, and K). The only additional species present in the explosives spectra were due to the substrate (Al I–II, AlO)

Wavelength/nm	Peak	RDX	TNT	Comp-B	Al	Dust	Oil	Fingerprint	AA	BG
247.890	C I	✘	✘	✘			✘	✘	✘	✘
833.715	C I	✘	✘	✘			✘	✘	✘	✘
467.752	C_2						✘			
468.370	C_2						✘			
469.656	C_2	✘	✘	✘			✘			
471.403	C_2	✘	✘	✘			✘			
473.608	C_2	✘	✘	✘			✘			
512.941	C_2	✘	✘	✘			✘			
516.351[a]	C_2						✘			
558.416	C_2						✘			
563.466	C_2						✘			
384.821	CN	✘	✘	✘			✘		✘	✘
385.205	CN	✘	✘	✘			✘		✘	✘
385.863	CN	✘	✘	✘			✘	✘	✘	✘
386.850	CN	✘	✘	✘			✘	✘	✘	✘
388.055	CN	✘	✘	✘			✘	✘	✘	✘
415.002	CN						✘			
415.592	CN						✘			
416.611	CN						✘			
417.898	CN						✘			
419.504	CN						✘			
421.428	CN						✘			
789.522	CN						✘		✘	✘
656.459	H I	✘	✘	✘	✘	✘	✘	✘	✘	✘
742.468	N I	✘	✘	✘	✘	✘	✘	✘	✘	✘
744.366	N I	✘	✘	✘	✘	✘	✘	✘	✘	✘
747.000	N I	✘	✘	✘	✘	✘	✘	✘	✘	✘
777.367	O I	✘	✘	✘	✘	✘	✘	✘	✘	✘
315.881	Ca II					✘		✘	✘	✘
317.946	Ca II					✘		✘	✘	✘
393.192	Ca II	✘	✘	✘		✘	✘	✘	✘	✘
422.550	Ca I	✘	✘	✘	✘	✘	✘	✘	✘	✘
766.516	K I	✘	✘	✘		✘	✘	✘	✘	✘
769.964	K I	✘	✘	✘		✘	✘	✘	✘	✘
589.041	Na I	✘	✘	✘		✘	✘	✘	✘	✘
589.709	Na I	✘	✘	✘		✘	✘	✘	✘	✘
818.282	Na I					✘	✘	✘	✘	✘

[a] The strongest C_2 line occurs at the edge of a spectrometer channel and appears only when the C_2 emission is extremely intense.

H/C > C_2/CN, H/C > (O + N)/(C + H), N/C > N/CN, N/C < (O + N)/(C + H), O/H > N/H, C/CN < H/CN, C/CN < C_2/CN, O/CN > N/CN, O/CN > (O + N)/(C + C_2 + CN + H), Ca/O < Ca/N, C < CN, C < O, N < O), the sample is classified as an explosive. The ratios were calculated by using summed background-corrected intensities of the C, C_2, CN, H, N, O, Ca, Na, and K lines present in the spectra (Table 2). The use of summed intensities rather than single peak intensities results in greater reproducibility among the single-shot spectra. The ratios were chosen such that all 150 of the pure RDX, TNT, and Composition-B (Comp-B) residue samples are classified as explosives using these criteria. In order to confirm the validity of the criteria for explosive samples, ST-LIBS spectra of an additional 26 RDX residue samples were acquired on a separate day several months later and were identified as explosives based on the 16 criteria above (0% false negatives).

Less than two percent of the interferent samples (Al, dust, oil, fingerprint, mold, BG) resulted in false positives using this algorithm. Four of the five misclassified spectra belonged to fingerprint residue samples (the other was BG). Unfortunately, the algorithm did not perform well for mixtures containing RDX. Only one of the RDX/dust mixture samples was correctly identified as an explosive (99% false negatives), although none of the oil/dust samples resulted in false positives. Despite its success with pure materials, a more sophisticated algorithm is clearly needed for real-world applicability.

Linear correlation is a simple measure of the strength of the relationship between two variables. ARL has successfully applied linear correlation to the discrimination of biomaterial powders detected on indoor surfaces using the MP-LIBS.[19] For the current experiment, a library of 50 spectra each (containing 8887 data points) of RDX, TNT, Al, dust, and oil was created and the correlation tool in the Analysis Toolpak of Microsoft Excel was used to test each of the RDX, TNT, Al, dust, and oil spectra individually against the library (the sample spectrum being tested was temporarily removed from the library for the calculation). The five library spectra with the highest correlation to the sample spectrum were identified based on the calculated correlation coefficients between the sample spectrum and each of the library spectra; the identity of the highest correlation match in the library was used to identify the sample spectrum.

Table 3 Results of linear correlation using entire spectra (50 spectra of each unknown were tested against a library containing either 49 or 50 spectra each of RDX, TNT, Al, dust, and oil. The 50 unknown samples of RDX, TNT, Al, dust, and oil were removed from the library one at a time and tested against the remaining spectra in the library

	Number of matches with the strongest correlation							
Unknown sample	RDX	TNT	Al	Dust	Oil	Correct ID (%)	False positives (%)	False negatives (%)
RDX	50	0	0	0	0	100	—	0
TNT	0	50	0	0	0	100	—	0
Aluminium	0	0	50	0	0	100	0	—
Arizona dust	0	0	0	50	0	100	0	—
Lubricant oil	0	0	0	0	50	100	0	—
Composition-B	11	39	0	0	0	100	—	0
Fingerprint residue	44	5[a]	1[b]	0	0	—	98	—
RDX/dust mix (acetone)	0	47	0	3	0	94	—	6
RDX/dust mix (crushed)	0	2	0	48	0	4	—	96
Oil/dust mix	0	0	0	50	0	—	0	—

[a] Three of the samples had Al ranked 2–5. [b] The sample had dust ranked 2–5.

The results of the highest correlation match generated using the entire broadband spectra are given in Table 3. Unless otherwise indicated in the table, the top five correlation matches in the library belonged to the same library class. All spectra of the five sample types included in the library (RDX, TNT, aluminium, dust, and oil) were correctly identified using this method, indicating that the sample spectra were reproducible for this data set. Sample types not included in the library were also compared to the library spectra. Comp-B residue spectra were tested against the library, which correctly identified all the samples as explosives (either RDX or TNT). Comparison of the fingerprint residues to the library resulted in a large number of false positives (98%), however. Linear correlation was able to correctly classify 94% of the RDX/dust (acetone) mixtures as explosives, but only 4% of the RDX/dust (crushed) samples were correctly classified.

A second library was constructed using nine summed peak intensities (C, C_2, CN, H, N, O, Ca, Na, and K) and 20 intensity ratios [O/C, H/C, O/N, N/C, O/H, N/H, C/CN, O/CN, H/CN, N/CN, C_2/CN, C_2/C, (O + N)/(H + C), Ca/H, Ca/C, Ca/O, Ca/N, (O + N)/(C + C_2 + CN + H), (O/N)/(H/C), and CN/(N/C)] rather than the entire spectra, which contain emission lines from the substrate in addition to those from the sample residue. The results of the linear correlation using the abbreviated data set are given in Table 4. As before, the top five correlation matches for each test sample with the library were determined, and the highest correlation match was used to identify the sample. The percentage of correct identifications using this method is lower for the RDX, Comp-B and the RDX/dust mixtures than those obtained using the entire spectra. Since the summed intensities and ratios reflect the composition of the sample residues, this means that the linear correlation using the entire spectra is dependent upon intensity information from the substrate/background to improve the classification of unknown samples. For this reason, linear correlation is unlikely to be effective for identifying residues on different substrates.

Principal components analysis (PCA) is a chemometric technique which finds combinations of variables that describe major trends in the data. PCA enables data compression and information extraction, and has previously been applied to LIBS spectra of bioagent simulants and interferents.[20] Preliminary results on explosives discrimination have also been presented.[12] A PCA model based on the values for the six ratios O/N, O/C, H/C, N/C, O/H, and N/H (calculated using the peak intensity of the strongest C, H, N and O lines) was developed and the resulting scores for the first three principal components are shown in Fig. 7. The PCA scores for each principal component represent weighted sums of the original variables. The first three principal components describe 65.24% (PC1), 25.06% (PC2), and 8.97% (PC3) of the total variance within the data set. A three-dimensional PCA scores

Table 4 Results of linear correlation using nine summed peak intensities (C, C_2, CN, H, N, O, Ca, Na, K) and 20 ratios (see text)

	Number of matches with the strongest correlation							
Unknown sample	RDX	TNT	Al	Dust	Oil	Correct ID (%)	False positives (%)	False negatives (%)
RDX	49	0	0	1	0	98	—	2
TNT	0	50	0	0	0	100	—	0
Aluminium	0	0	50	0	0	100	0	—
Arizona dust	0	0	0	50	0	100	0	—
Lubricant oil	0	0	0	0	50	100	0	—
Composition-B	32	17	0	0	1[a]	98	—	2
Fingerprint residue	38	7	3	2	0	—	90	—
RDX/dust mix (acetone)	16	6	1	27	0	44	—	56
RDX/dust mix (crushed)	0	0	0	50	0	0	—	100
Oil/dust mix	0	0	0	50	0	—	0	—

[a] TNT was ranked 5th.

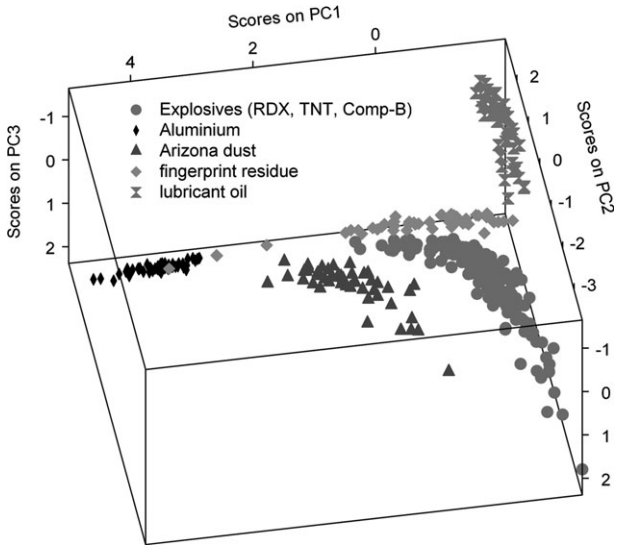

Fig. 7 PCA scores plot of explosive residues and interferents (50 samples each) constructed using the ratios O/N, O/C, H/C, N/C, O/H, and N/H. The strongest emission lines for each element (C 247 nm, H 656 nm, N 747 nm, and O 777 nm) were used for the background-corrected peak intensities. The explosive residues (RDX, TNT, Comp-B) overlap with each other, but form an isolated group separate from the interferent groups. No overlap exists between any of the groups using the first three principal components, except for several of the fingerprint residues that group near the blank aluminium substrate samples (indicating that the plasma sampled an area without any detectable fingerprint residue).

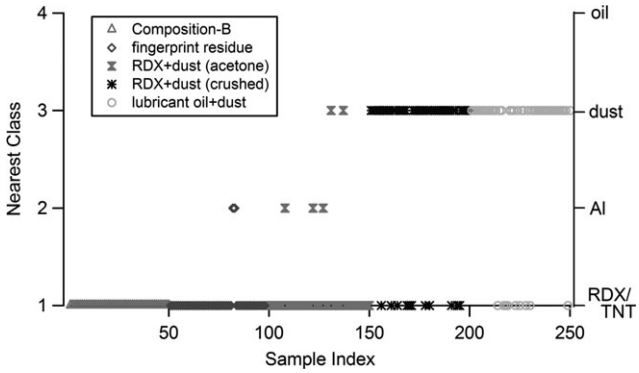

Fig. 8 Results of 'unknown' samples (50 each) of Comp-B, fingerprint residue, RDX/dust mixed in acetone and deposited on the aluminium substrate, RDX/dust crushed directly on the aluminium, and oil/dust smeared on aluminium tested against a SIMCA model built using 50 spectra each (represented by nine summed peak intensities and 20 ratios) of RDX and TNT (class 1), aluminium (class 2), Arizona dust (class 3), and lubricant oil (class 4). The SIMCA model predicted the nearest class of the unknown sample based on the known samples in the model. Most of the fingerprint residue samples and several of the oil/dust samples were incorrectly classified as explosives (false positives), while a significant number of the RDX/dust samples were classified as dust rather than RDX (probable false negatives).

plot shows the separation of the different samples based on the six ratios.

The three explosive residues (RDX, TNT, and Comp-B) group together using this model but are isolated from the interferent sub-groups. No overlap exists between any of the interferent groups, although several of the fingerprint residues group near the blank aluminium substrate samples (indicating that the plasma sampled an area without any detectable fingerprint residue). A closer look at the loadings for the principal components shows that the O/N and H/C ratios load most significantly into PC1 and are anti-correlated. PCA thus provides a useful tool for identifying whether samples are the same or different and what variables are responsible for the differences. This PCA model could also be used to classify a sample as explosive or non-explosive depending on whether the unknown sample groups with the other explosives.

Even greater sample group separation can be achieved by making use of the broadband nature of the acquired LIBS spectra. Using the nine summed intensities and 20 ratios discussed earlier should provide much better separation between the sample sets. In order to account for greater than 99% of the variance using PCA with the 29 variables (as in the first example using six variables and three principal components), 13 principal components are needed. The sample separations are therefore difficult to visualize in two or three dimensions.

An alternative approach is to use the soft independent method of class analogy (SIMCA), which consists of a collection of PCA models, one for each class in the data set. Each PCA model has an independently determined number of principal components (PC) that describe the variance within the class. The SIMCA model can then be used to determine the nearest class for unknown samples. A SIMCA model was built using 50 spectra each (represented by nine summed peak intensities and 20 ratios) of RDX and TNT (class 1, 8 PC), aluminium (class 2, 5 PC), Arizona dust (class 3, 7 PC), and lubricant oil (class 4, 8 PC). 'Unknown' samples (50 each) of Comp-B, fingerprint residue, RDX/dust (acetone), RDX/dust (crushed), and an oil/dust mixture were then tested against the model. The results of these tests are shown in Fig. 8. Although the model correctly classified all of the Comp-B samples and many of the RDX/dust samples as explosives, most of the fingerprint residue samples and several of the oil/dust samples were incorrectly classified as explosives (false positives). The main disadvantage of SIMCA is that the PCA models are computed with the goal of capturing intraclass variations without consideration of interclass differences.

Partial least squares discriminant analysis (PLS-DA) is a multivariate inverse least squares discrimination method used to classify samples. Unlike SIMCA, partial least squares generates predictor variables (called latent variables, LV) while attempting to capture variance and achieve correlation. The model predicts the class number for each sample based on a value of zero to one. A value closer to zero indicates that the sample is not in the modeled class, while a value of one indicates that the sample is in the modeled class. A threshold between zero and one (above which a sample is considered in the class) is automatically calculated by the software using Bayesian statistics in order to minimize the number of false positives and false negatives. In practice, the predicted *Y*-values are not discrete zeros and ones but range from around zero to around one in a continuous manner. The number of

LV chosen to be included in each of the models described below was confirmed using cross-validation (leaving one out) to minimize the root-mean-square error.

The choice of data set to represent each spectrum was critical for enhancing the classification ability of the PLS-DA model. Using the entire broadband spectrum for constructing the model worked extremely well for the samples built into the model, but unknown samples not belonging to the original model were predicted to belong to each of the classes in the model with roughly equal probability. Different combinations of intensities and/or ratios based on peak intensities (or areas) of single lines or summed intensities of species found in the explosives spectra C, H, N, O, C_2, CN, and the impurities Ca, Na, and K were tested. The combination of nine summed intensities and 20 ratios previously described was found to provide the best discrimination for all the PLS-DA models based on our data set. Models built using only the nine summed intensities or just the 20 ratios performed nearly as well (with a few false positives and false negatives that do not occur when both intensities and ratios are used).

Fig. 9 demonstrates discrimination of the RDX, TNT, and Comp-B residues using PLS-DA. A PLS-DA model based on nine summed peak intensities and 20 ratios from 40 spectra of each residue type was developed (18 LV). A test set of 10 spectra from each residue type was used as the prediction set.

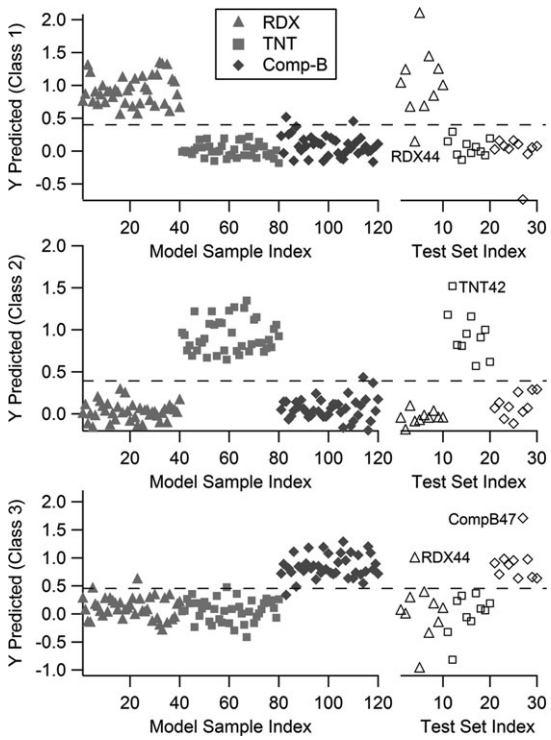

Fig. 9 Discrimination of different explosive residues using PLS-DA. Fifty spectra of RDX, TNT, and Comp-B (63% RDX, 36% TNT, 1% wax) on aluminium were acquired and a PLS-DA model based on nine summed peak intensities and 20 ratios was developed using 40 spectra of each residue. An additional ten spectra of each residue type were used as the prediction set. Excellent discrimination of the samples was achieved, although some overlap between the RDX and Comp-B occurs due to the high percentage of RDX in Comp-B.

Excellent discrimination of the explosive samples was achieved (using the Bayesian thresholds shown in the figure), although some overlap between the RDX and Comp-B occurs in the model due to the high percentage of RDX in Comp-B. All but one of the prediction samples was correctly classified (one RDX sample was classified as Comp-B). These results show that discrimination of different types of explosives is possible using LIBS, despite their similar molecular structures (Table 1).

When the explosive, aluminium, dust, oil, and fingerprint residue spectra (50 spectra each) were used to create a PLS-DA model with 17 LV based on the nine summed peak intensities and 20 ratios, nearly perfect classification of the samples was achieved within the model (Fig. 10). Two fingerprint residue samples were predicted to belong to the same class as aluminium – a visual inspection of those spectra confirm that no carbon and very little hydrogen are present, indicating that the plasma most likely sampled an area that contained no fingerprint residue. Because application of the fingerprint residue to the aluminium resulted in channels of residue corresponding to the ridges of a human fingerprint, this result is not too surprising. In addition, one of the aluminium samples was predicted to be a fingerprint residue.

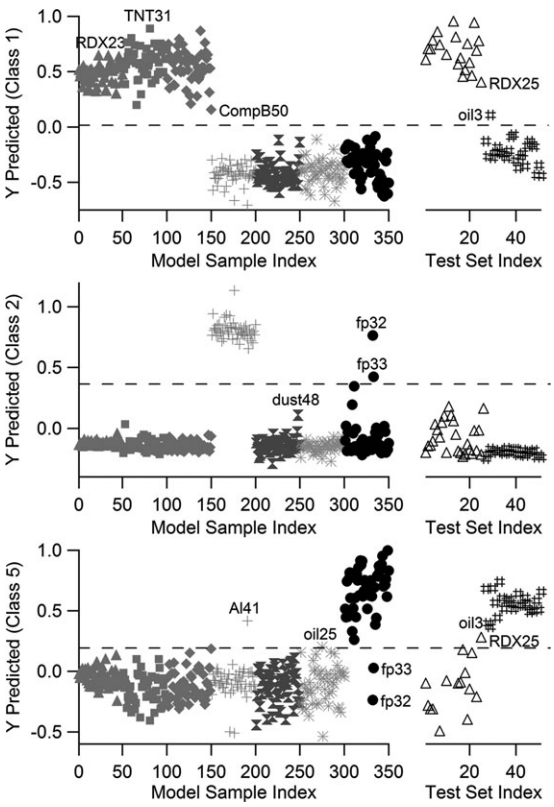

Fig. 10 PLS-DA model showing the classification of samples using nine summed intensities and 20 ratios. All explosive (class 1), dust (class 3), and oil (class 4) samples in the model class correctly. Fingerprint residues #32 and #33 group with aluminium as class 2 (visual inspection of the spectra confirm that the plasma did not sample a detectable amount of residue); Al #41 most likely contained some fingerprint residue (class 5). All 26 RDX residue samples in the prediction set correctly classify as explosives, although one oil residue sample in the prediction set results in a false positive.

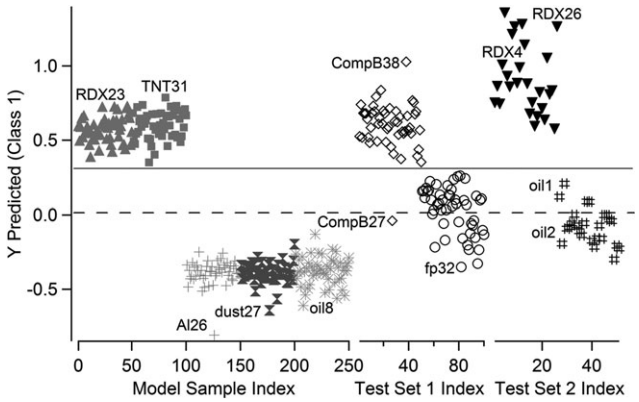

Fig. 11 PLS-DA model built on RDX, TNT, Al, dust, oil (20 LV). 'Unknown' samples of Comp-B (50 spectra) and fingerprint residue (50 spectra) were applied to the model (test set 1) to test how well the model handles substances not in the model. With a user-specified threshold (solid line), Comp-B was correctly identified as an explosive (with the exception of one sample) and the fingerprints were identified as non-explosives (classified as oil, aluminium, or dust). A second test set consisting of additional RDX residue spectra (26) and oil residue spectra (25) was applied to the model to determine the validity of the user-specified threshold.

It is quite possible that the plasma sampled an area of the aluminium accidentally contaminated with fingerprints.

When an additional 26 RDX residue and 25 oil residue spectra acquired from samples prepared several months later were tested against the model, all of the RDX and one of the oil samples were classified as explosives. Removing the suspect fingerprint (#32 and #33) and aluminium (#41) samples from the model did not affect the test set results. The oil residue samples from the test set classified with the fingerprints as well as with the oil in the model (Fig. 10). Because the laser interacts more weakly with the liquid oil than the aluminium substrate, differences in the amount of surface coverage for the oil residue samples affect the plasma temperature and therefore the intensity ratios. Including a variety of residue concentrations in the model classes will help improve the prediction ability of the model.

Despite the encouraging success of PLS-DA for classifying explosive residues, for real-world applications it would be impossible to include every possible interferent in the model. In order to test the ability of PLS-DA to deal with samples (explosive and non-explosive) not included in the original model, a model was developed based on RDX, TNT, Al, dust, and oil (20 LV, 50 spectra each). The spectra of Comp-B and fingerprint residue (test set 1) were then tested against this model, which predicted the classification of the 'unknown' samples (Fig. 11). Using the Bayesian threshold calculated by the PLS_Toolbox (on the model data only), a significant number of the fingerprint residues register as false positives. Because the position of the threshold can be selected based on the number of false positives and false negatives the user is willing to accept, the threshold can be chosen as shown in Fig. 11 (solid line) such that all but one of the Comp-B samples and none of the fingerprint residues register as explosives. The remainder of the fingerprint residue samples are classified by the model as either oil (11 samples), aluminium (4 samples), or dust (3 samples) according to the Bayesian thresholds. To test the validity of the new user-selected threshold for future predictions, an additional 26 RDX and 25 oil residue spectra (prepared on a separate day several months later) were tested against the model (test set 2 in Fig. 11). All of the new test samples were correctly classified as either explosive or non-explosive with the previously determined user-selected threshold.

Table 5 Classification results of mixtures of RDX/dust (suspended in acetone or crushed directly on the substrate, 50 samples each) and oil/dust (50 samples) tested against a PLS-DA model built on RDX, aluminium, and Arizona dust

	Unknown samples		
Model class	RDX/dust (acetone) (%)	RDX/dust (crushed) (%)	Oil/dust (%)
RDX	100	66	0
Aluminium	0	0	0
Arizona dust	24	100	100

Another important issue in real-world applications is the ability of the model to recognize explosives in the presence of interferents. A PLS-DA model based on RDX, Al, and dust was created using the nine summed intensities and 20 ratios (6 LV, 50 spectra each). The RDX/dust mixtures (suspended in acetone or crushed directly on the aluminium) and the oil/dust mixture spectra were then tested against the model. All of the RDX/dust (acetone) samples and more than half of the RDX/dust (crushed) samples were classified as RDX (Table 5). Because the RDX/dust (crushed) samples were extremely inhomogeneous, it is likely that the RDX/dust samples identified by the model as non-explosives contained only dust and thus were correctly classified. Many of the RDX/dust samples were also classified with the pure dust samples. The oil/dust mixture grouped only with the pure dust since pure oil was not included in the model, and did not result in any false positives. These results demonstrate the applicability of this explosive/non-explosive classification method to mixtures.

Finally, a PLS-DA model was constructed using RDX, TNT, Al, dust, oil, mold (AA), and BG (20 LV, 50 spectra each) based on summed intensities for C, N, O, H, C_2, CN, Ca, Na, K, Ba, Li, Mg, Mn, Sc, Si, and Sr, and 23 intensity ratios [O/C, H/C, O/N, N/C, O/H, N/H, C/CN, O/CN, H/CN, N/CN, C_2/CN, C_2/C, (O + N)/(H + C), Ca/H, Ca/C, Ca/O, Ca/N, (O + N)/(C + C_2 + CN + H), (O/N)/(H/C), CN/(N/C), Mg/Mn, Si/Li, (Sr + Sc)/Ba]. The intensities and ratios were chosen based on the peaks present in the LIBS spectra of the hazards of interest, explosives and the anthrax surrogate BG. Table 6 lists the lines observed in the bio-residue spectra, including those used for the summed intensities.

The correct explosive/non-explosive classification of the 'unknown' Comp-B and fingerprint samples (with a user-defined threshold as before) together with the correct classification of the test anthrax surrogate samples (five additional BG samples not included in the model) demonstrates that simultaneous biohazard and explosive residue discrimination is possible using standoff LIBS (Table 7). Although 88% of the fingerprint residue samples classified as mold, the important

Table 6 Lines from the biomaterials spectra *Alternia alternata* (AA) and *Bacillus subtilis* (BG) on aluminium (excluding lines present in the spectra of the aluminium substrate)

Wavelength/nm	Peak	AA	BG	Wavelength/nm	Peak	AA	BG	Wavelength/nm	Peak	AA	BG
363.036	?		✘	558.977	Ca I	✘	✘	260.584[a]	Mn II		✘
364.372	?		✘	559.539	Ca I	✘	✘	293.324[a]	Mn II		✘
383.778	?	✘	✘	585.926	Ca I	✘	✘	293.930[a]	Mn II		✘
455.383[a]	Ba II	✘	✘	610.431	Ca I	✘	✘	294.922[a]	Mn II		✘
493.421[a]	Ba II	✘	✘	612.308	Ca I	✘	✘	353.144[a]	Mn I		✘
553.694	Ba I		✘	616.389	Ca I	✘	✘	354.734[a]	Mn I		✘
247.890[a]	C I	✘	✘	617.050	Ca I	✘	✘	356.903[a]	Mn I		✘
833.715[a]	C I	✘	✘	644.036	Ca I	✘	✘	401.784[a]	Mn I		✘
315.881[a]	Ca II	✘	✘	645.128	Ca I	✘	✘	405.52[a]	Mn I		✘
317.946[a]	Ca II	✘	✘	646.328	Ca I	✘	✘	408.274[a]	Mn I		✘
370.648	Ca II	✘	✘	647.310	Ca I	✘	✘	475.400[a]	Mn I		✘
373.693	Ca II	✘	✘	649.491	Ca I	✘	✘	476.218[a]	Mn I		✘
393.192[a]	Ca II	✘	✘	650.036	Ca I	✘	✘	476.576[a]	Mn I		✘
396.951	Ca II	✘	✘	671.859	Ca I	✘	✘	478.312[a]	Mn I		✘
422.657[a]	Ca I	✘	✘	714.906	Ca I	✘	✘	482.337[a]	Mn I		✘
428.249	Ca I	✘	✘	720.334	Ca I	✘	✘	330.220	Na I	✘	✘
428.887	Ca I	✘	✘	732.747	Ca I	✘	✘	498.195	Na I	✘	✘
430.214	Ca I	✘	✘	388.219[a]	CN	✘	✘	568.956	Na I	✘	✘
430.745	Ca I	✘	✘	418.005[a]	CN	✘	✘	589.041[a]	Na I	✘	✘
431.805	Ca I	✘	✘	419.611[a]	CN	✘	✘	589.597[a]	Na I	✘	✘
435.563	Ca I	✘	✘	438.308	Fe I	✘	✘	818.385[a]	Na I	✘	✘
442.520	Ca I	✘	✘	656.459[a]	H I	✘	✘	819.512	Na I	✘	✘
443.465	Ca I	✘	✘	766.516[a]	K I	✘	✘	409.569[a]	Sc I		✘
445.460	Ca I	✘	✘	769.964[a]	K I	✘	✘	409.838[a]	Sc I		✘
457.877	Ca I		✘	670.885[a]	Li I	✘	✘	634.520[a]	Sc I		✘
458.137	Ca I		✘	277.979[a]	Mg I	✘	✘	636.273[a]	Sc I		✘
487.816	Ca I		✘	279.537[a]	Mg II	✘	✘	251.623[a]	Si I		✘
504.197	Ca I		✘	280.259[a]	Mg II	✘	✘	288.188[a]	Si I		✘
518.854	Ca I		✘	285.198[a]	Mg I	✘	✘	403.085[a]	Sr I		✘
526.579	Ca I	✘	✘	517.262[a]	Mg I	✘	✘	407.735[a]	Sr II		✘
527.033	Ca I		✘	518.399[a]	Mg I	✘	✘	458.604[a]	Sr II		✘
534.965	Ca I		✘	631.890	Mg ?		✘	460.729[a]	Sr I		✘
551.331	Ca I		✘	259.403[a]	Mn II		✘	640.868[a]	Sr I		✘

[a] Lines used to give summed peak intensities for C, N, O, H, C_2, CN, Ca, Na, K, Ba, Li, Mg, Mn, Sc, Si, and Sr.

Table 7 Classification results of 'unknown' composition-B (50 samples), fingerprint residue (50 samples), and *Bacillus subtilis* (BG, 5 samples) tested against a PLS-DA model built on RDX, aluminium, Arizona dust, oil, mold (*Alternia alternata*, AA), and BG

	Unknown samples		
Model class	Composition-B (%)	Fingerprint residue (%)	BG (%)
RDX	100	0	0
Aluminium	0	8	0
Arizona dust	0	0	0
Oil	0	2	0
Mold (AA)	0	88	0
BG	0	0	100

result is that they did not classify as explosives despite the fact that the fingerprint residue was not included in the original model. If the user was interested in identifying mold, peak intensities and ratios based on mold would be used to construct the model.

Conclusions

Recent work at ARL demonstrates the importance of eliminating the oxygen and nitrogen contribution from air for sensitive and selective LIBS detection of explosive residues. An argon flow can be used to displace air for close-contact explosive residue detection (*e.g.* MP-LIBS), while collinear double-pulse LIBS works well for standoff detection of explosive residues (*e.g.* ST-LIBS). Despite the typical characterization of LIBS as an elemental technique, the relative elemental intensities in the LIBS spectra are representative of the stoichiometry of the parent molecules and can be used to discriminate materials containing the same elements.

We have shown that PLS-DA is able to discriminate among explosive and non-explosive sample spectra acquired at 20 m and can correctly classify samples not contained in the original model. The use of summed intensities and ratios from species observed in the explosives spectra enables the identification of explosive residues even when mixed with dust. In future studies we will apply spectra acquired under different conditions (standoff distance, laser power, substrate, *etc.*) to our model. The model will also be expanded to include different types of explosives and explosive mixtures as well as biological and chemical threats. Since all elements emit light in the UV-VIS-NIR region, the results in Table 7 demonstrate that broadband LIBS presents a significant advantage over other sensor technologies which can only detect very specific molecules.

Acknowledgements

Funding from the Office of the Secretary of Defense (OSD), the Department of Homeland Security (DHS), and the

Defense Emergency Relief Fund (DERF) is gratefully acknowledged. J. L. G. is supported by a US Army Research Laboratory Postdoctoral Fellowship administered by Oak Ridge Associated Universities.

References

1 *Detection of Explosives for Commercial Aviation Security*, National Research Council Committee on Commercial Aviation Security, Commission on Engineering and Technical Systems, National Academies Press, Washington, DC, 1993, http://www.nap.edu/catalog/2107.html (accessed 16 October 2007).

2 J. E. Parmeter, 'The challenge of standoff explosives detection, ', in *38th Annual International Carnahan Conference on Security Technology*, IEEE, Albuquerque, NM, 2004, pp. 355–358, DOI: 10.1109/CCST.2004.1405418.

3 J. F. Federici, B. Schulkin, F. Huang, D. Garyl, R. Barat, F. Oliveira and D. Zimdars, *Semicond. Sci. Technol.*, 2005, **20**, S266–S280.

4 J. I. Steinfeld and J. Wormhoudt, *Annu. Rev. Phys. Chem.*, 1998, **49**, 203–232.

5 G. L. Gresham, J. P. Davies, L. D. Goodrich, L. G. Blackwood, B. Y. H. Liu, D. Thimsem, S. H. Yoo and S. F. Hallowell, *Proc. SPIE-Int. Soc. Opt. Eng.*, 1994, **2276**, 34–44.

6 C. A. Munson, J. L. Gottfried, F. C. De Lucia, Jr, K. L. McNesby and A. W. Miziolek, 'Laser-Based Detection Methods for Energetic Materials, ', in *Counterterrorist Detection Techniques for Explosives*, ed. J. Yinon, Elsevier, Amsterdam, 2007, pp. 279–321.

7 S. K. Sharma, A. K. Misra and B. Sharma, *Spectrochim. Acta, Part A*, 2005, **61**, 2404–2412.

8 J. C. Carter, S. M. Angel, M. Lawrence-Snyder, J. Scaffidi, R. E. Whipple and J. G. Reynolds, *Appl. Spectrosc.*, 2005, **59**, 769–775.

9 F. C. De Lucia, Jr, R. S. Harmon, K. L. McNesby, R. J. Winkel, Jr and A. W. Miziolek, *Appl. Opt.*, 2003, **42**, 6148–6152.

10 R. S. Harmon, F. C. De Lucia, Jr, A. LaPointe, R. J. Winkle, Jr and A. W. Miziolek, *Proc. SPIE-Int. Soc. Opt. Eng.*, 2005, **5794**, 92–101.

11 F. C. De Lucia, Jr, A. C. Samuels, R. S. Harmon, R. A. Walters, K. L. McNesby, A. LaPointe, R. J. Winkel, Jr and A. W. Miziolek, *IEEE Sensors J.*, 2005, **5**, 681–689.

12 J. L. Gottfried, F. C. De Lucia, Jr, C. A. Munson and A. W. Miziolek, *Spectrochim. Acta, Part B*, LIBS2006 special issue, in the press.

13 F. C. De Lucia, Jr, J. L. Gottfried, C. A. Munson and A. W. Miziolek, *Spectrochim. Acta, Part B*, LIBS2006 special issue, in the press.

14 R. S. Harmon, F. C. De Lucia, Jr, C. A. Munson, A. W. Miziolek and K. L. McNesby, *Proc. SPIE-Int. Soc. Opt. Eng.*, 2005, **5994**, 59940K/1–7.

15 R. S. Harmon, F. C. De Lucia, Jr, A. LaPointe, R. J. Winkle, Jr and A. W. Miziolek, *Anal. Bioanal. Chem.*, 2006, **385**, 1140–1148.

16 R. S. Harmon, F. C. De Lucia, Jr, A. LaPointe and A. W. Miziolek, *Proc. SPIE-Int. Soc. Opt. Eng.*, 2006, **6217**, 62140I/1–7.

17 V. I. Babushok, F. C. DeLucia, Jr, J. L. Gottfried, C. A. Munson and A. W. Miziolek, *Spectrochim. Acta, Part B*, 2006, **61**, 999–1014.

18 C. Lopez-Moreno, S. Palanco, J. Javier Laserna, F. C. De Lucia, Jr, A. W. Miziolek, J. Rose, R. A. Walters and A. I. Whitehouse, *J. Anal. At. Spectrom.*, 2006, **21**, 55–60.

19 C. A. Munson, J. L. Gottfried, F. C. De Lucia, Jr and A. W. Miziolek, 'LIBS analysis of Hazardous Materials on Indoor Surfaces, ', poster presentedat LIBS2006, Montréal, Qc, Sept. 5–8, 2006.

20 C. A. Munson, F. C. De Lucia, Jr, T. Piehler, K. L. McNesby and A. W. Miziolek, *Spectrochim. Acta, Part B*, 2005, **60**, 1217–1224.

